YIELD STRESS FLUID FLOW PAST A CIRCULAR CYLINDER CONFINED IN A CHANNEL

NGHIÊN CỨU DÒNG CHẢY LƯU CHẤT CÓ TÍNH ỨNG SUẤT TỚI HẠN QUA TRỤ TRÒN ĐẶT TRONG KÊNH

Son Thanh Nguyen, Anh-Ngoc Tran Ho*, Cuong Mai Bui*

The University of Danang - University of Technology and Education

*Corresponding authors: htangoc@ute.udn.vn; bmcuong@ute.udn.vn

(Received: August 18, 2022; Accepted: November 02, 2022)

Abstract - This paper presents a numerical investigation of flow characteristics of yield stress fluid over a confined cylinder at Re=50-100. Sediment suspension with kaolinite mass concentration from c=15-28.5% are targeted. To describe the yield stress effect, the Bingham-Papanastasiou model is utilized. Various flow features of the yield stress fluid, i.e., formation of solid-like regions, streamlines, vorticity distribution, and drag force are reported and analyzed. In detail, the suspension flow is found to be steady within the condition range studied. With a very large kaolinite fraction (i.e., c=28.5%), the flow is in a creeping mode without downstream circulation developed. Moreover, solid-like regions are found to be greatly affected by the Reynolds number and yield stress effect. Additionally, the flow behaviors confined in a channel are significantly different from those produced by the unconfined one (infinite blockage). Furthermore, the drag coefficient is found to strongly depend on Reynolds number and kaolinite fraction.

Key words - yield stress; non-Newtonian; sediment flow; CFD

Tóm tắt – Bài báo trình bày nghiên cứu dòng chảy lưu chất có tính ứng suất tới hạn qua trụ tròn bị giới hạn tại Re=50-100. Huyền phù trầm tích có nồng độ khối lượng c=15-28,5% được khảo sát. Phương pháp Bingham-Papanastasiou được sử dụng để mô hình hóa đặc tính ứng suất tới hạn. Nhiều kết quả về hành vi thủy động của lưu chất có tính ứng suất tới hạn như sự hình thành vùng rắn, đường dòng, phân bố xoáy, và lực cản được báo cáo và phân tích. Cụ thể, dòng chảy ở chế độ ổn định trong toàn bộ điều kiện khảo sát. Với nồng độ kaolinite lớn (ví dụ: c=28,5%), dòng chảy thậm chí ở chế độ chảy leo; các vùng xoáy không được tìm thấy ở hạ lưu. Hơn nữa, các vùng rắn được xác định bị ảnh hưởng đáng kể bởi số Re và hiệu ứng ứng suất tới hạn. Thêm vào đó, đặc tính dòng chảy bị giới hạn bởi kênh có sự khác biệt lớn với trường hợp không bị giới hạn. Lực cản cũng được xác định phụ thuộc rất lớn vào số Re và nồng độ kaolinite.

Từ khóa – Ứng suất tới hạn; phi Newton; huyền phù; CFD

1. Introduction

Yield stress is one of the most important features of non-Newtonian fluid; with this characteristic, the material only flows once the applied shear stress outreaches a threshold value (i.e., yield stress), if not, they perform as a solid block. Typical examples of the yield stress liquid range from natural fluids such as mud, lava, or clay suspensions [1-3] to engineering ones such as fresh concrete, printing inks, oil, and polymer [4-7]. The hydrodynamic behaviors of such fluids are different from the Newtonian ones and have been not fully investigated yet.

Confined flows over a bluff body are frequently encountered in engineering applications, e.g., underwater installation, biostructure, and heat exchanger design. For Newtonian fluids, this problem is well investigated. For example, Chakraborty et al. [8], Sahin and Owens [9], and Singha and Singhamahapatra [10] studied wall proximity effects on the confined flow at Re≤280. It was found that the blockage ratio strongly affected the flow field behaviors, i.e., downstream circulation, vortex distribution and separation angle, and the hydrodynamic forces acting on the cylinder. For non-Newtonian fluids, the available works are mainly on the unconfined flow. For instance, Tokpavi et al. [11, 12] investigated a creeping flow of yield stress fluid using simulations and Particle Image Velocimetry (PIV) measurement technique. The fluid was at high Oldroyd numbers, $Od=\tau_0 D^n/Ku_0^n$ with τ_0 the yield stress, D the characteristic length, K the plastic viscosity, u_0 the velocity and n the power-law index, indicating the predominance of plastic effects over viscous ones. It was interesting to observe that solid-like zones were developed in high-viscosity regions. The size and shape of these zones were relevant to Od; in detail, the higher Od, the larger rigid zones were detected on the cylinder's surface and/or scattered in the flow field pattern. At non-zero Re, Mossaz et al. [13, 14] conducted massive numerical studies on viscoplastic fluids at Re≤100. Flow morphologies and hydrodynamic forces were reported and analyzed in detail. Furthermore, the viscoplastic characteristics were seen to stabilize the flow; specifically, since Od was also high, the flow remained in a stationary laminar regime at relatively high Re.

The work on the confined flow of non-Newtonian fluid is very few. Bharti and Chhabra [15] investigated a power-law fluid in a steady regime with a blockage ratio of $1.1\leq\beta\leq4$. Results for drag and pressure forces were found to be dependent on Re, power index, and β. Especially, the confining channel walls were determined to stabilize the flow with n<1 (shear-thickening liquid) or destabilize it with n>1 (shear-thinning liquid). This was in line with Bijjam and Dhiman [16], who numerically studied the time-dependent behaviors of power-law fluid at Re=50-150 and β=4. Zisis and Mitsoulis [17] and Mitsoulis [18] conducted simulations for a viscoplastic fluid, which was of Bingham type, over a confined cylinder at wide conditions of Bn and β. It was reported that the size, shape, and location of unyielded/yielded zones, and the drag acting on the cylinder strongly

depended on Bn and β. Experimental study on the confined non-Newtonian fluid flows is, however, not available to our best knowledge.

It is noteworthy that the available work for the confined yield stress fluid flow was only in a creeping mode (Re~0) where the inertia was negligible. In this work, the interest is in a more industrially applicable range of Re, i.e., Re=50-100. The cylindrical geometry is considered for the bluff body. Non-Newtonian yield stress effect is described with using properties of sediment suspension.

2. Theory background

2.1. Governing Equations

Continuity and momentum equations for a flow in a steady regime are expressed as follows,

$$\nabla \cdot \underline{u} = 0, \tag{1}$$

$$\rho \underline{u} \cdot \nabla \underline{u} = \rho \underline{f} + \nabla \cdot \underline{\underline{\sigma}}. \tag{2}$$

Here, $\underline{u}$ and $\underline{f}$ are the velocity and body force vectors, respectively; ρ is the fluid density. The total stress tensor is

$$\underline{\underline{\sigma}} = -p\underline{\underline{I}} + \underline{\underline{\tau}} \tag{3}$$

with p being the pressure, $\underline{\underline{I}}$ the unit tensor, $\underline{\underline{\tau}} = 2\mu\underline{\underline{\dot{\gamma}}}$ the deviatoric stress tensor, and $\underline{\underline{\dot{\gamma}}}$ the deformation rate tensor.

2.2. Fluids and Rheological Model

In this work, the yield stress fluid is sediment suspension with kaolinite mass fraction varying from c=15-28.5%. Mixture properties of kaolinite clay were reported in Lin et al. [19]. It is noticed that the higher the kaolinite fraction, the larger the yield stress of the suspension, and then the greater yield stress/viscoplastic effects.

The Bingham model is utilized to express the yield stress behavior of the fluid investigated as follows,

$$\begin{cases} \underline{\underline{\tau}} = \left(K + \dfrac{\tau_0}{\dot{\gamma}} \right) \underline{\underline{\dot{\gamma}}} & if\ \tau > \tau_0 \\ \dot{\gamma} = 0 & if\ \tau \le \tau_0 \end{cases}. \tag{4}$$

Here, τ is the intensity of extra-stress and $\dot{\gamma}$ the strain rate tensor's magnitude. It is noted that the estimation approach for K can be referred to [20]. Reynolds (Re) and Bingham (Bn) are two non-dimensional numbers desribing the flow condition, as follows,

$$\mathrm{Re} = \frac{\rho u_0 D}{K}, \tag{5}$$

$$Bn = \frac{\tau_0 D}{K u_0}, \tag{6}$$

The former determines the inertial effect meanwhile the latter characterizes the viscoplastic one of the fluid flow. Herewith, u_0 being the incoming velocity and D the cylinder's diameter.

3. Computational approach

3.1. Regularization scheme

It is noted that the discontinuity in Bingham model can result in numerical errors; to tackle this, the Papanastasiou's regularization is employed as [21]:

$$\underline{\underline{\tau}} = \left(K + \frac{\tau_0 (1 - \mathrm{e}^{-m\dot{\gamma}})}{\dot{\gamma}} \right) \underline{\underline{\dot{\gamma}}}, \tag{7}$$

With m the regularization parameter. When m is very large, i.e., $m \to \infty$, the curve of Eq. (7) approaches the bi-viscosity one of Eq. (4).

3.2. Computational Domain

The problem geometry is presented in Figure 1. In detail, a two-dimensional (2D) cylinder is placed inside a channel. The channel height is H, and its downstream length is of L_2=7.5H. To better predict the flow field behaviors over a confined cylinder, it is necessary to ensure that the entrance length L_1 is sufficient for the full flow development. To do this, simulations with the straight channel flow (without the cylinder) are performed to determine the position where it reaches fully developed.

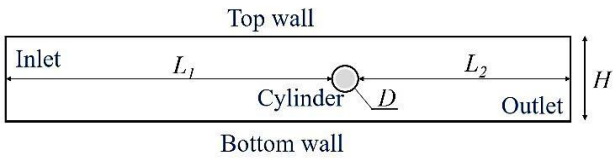

Figure 1. *Problem geometry*

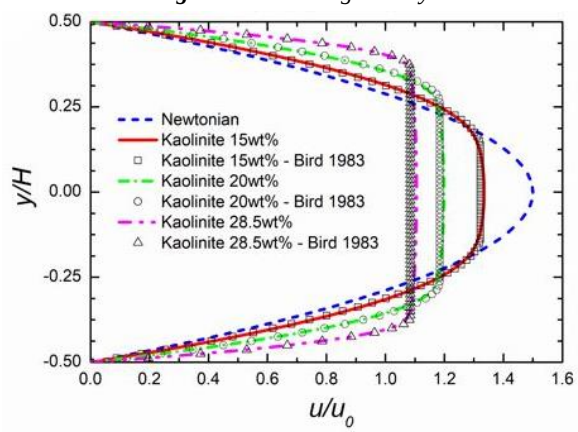

Figure 2. *Fully-developed velocity profiles with various kaolinite fraction at Re_H=400*

Results for the fully-developed profiles at Re_H = 400 are shown in Figure 2 ($Re_H=\rho u_0 H/K$). Different from the parabolic curve of a Newtonian fluid, due to the small shear rate at the channel core, a plateau perpendicular to the channel's horizontal centerline is formed in yield stress fluid profiles. This zone, which is called a plug region, is larger with the increasing kaolinite mass fraction. Importantly, our results have very good agreement with the analytical solution of Bird et al. [22], possibly showing reliable findings for the full-development position.

The position for the full flow development is considered as the one the velocity reaches 99% of the steady value [23]. With this, our results for the entrance-

length at Re_H=400 are s/H=18, 9.8, 3.4, and 0.6 for, respectively, Newtonian fluid, kaolinite 15%, 20%, and 28.5%. As can be observed, the higher kaolinite fraction, the greater distance that the flow requires to be fully developed. We then select the upstream length of L_1=12.5H ensuring the full development of yield stress fluid flow at the largest Re investigated in this work (i.e., Re=100 corresponding Re_H=400).

For the boundary conditions, we apply a constant velocity (u_0) at the inlet, the atmosphere pressure at the outlet, and the no-slip stationary condition for the top wall, bottom wall, and the cylinder's surface.

3.3. Computational Mesh

A structured finite volume mesh with a high resolution near the cylinder and channel walls is created (see Figure 3).

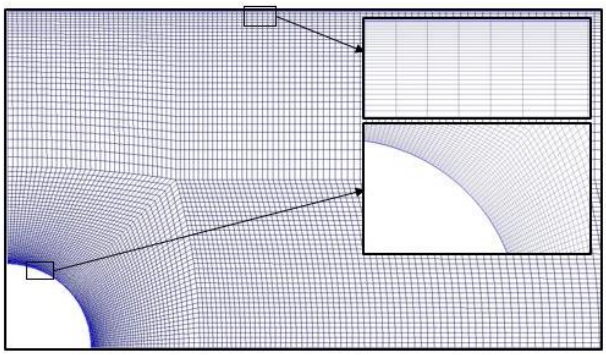

Figure 3. *Near-field structured mesh*

Table 1. *Mesh sensitivity study for drag coefficient at re=100*

Mesh	Newtonian		Kaolinite 20%	
	C_d	Running Time (min.)	C_d	Running Time (min.)
42K	2.89	16	2.92	33
62K	2.87	20	2.91	43
85K	2.87	25	2.91	68

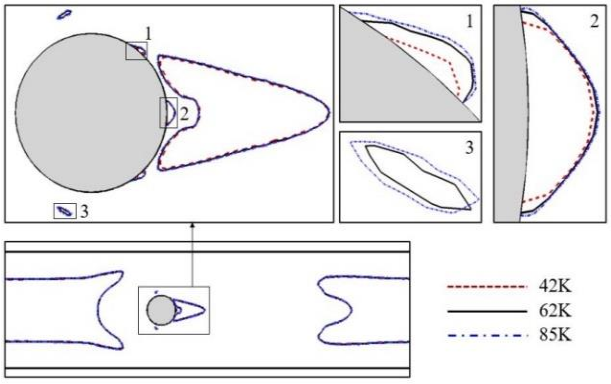

Figure 4. *Mesh sensitivity study for yield surface of kaolinite 20% at Re=100*

A mesh sensitivity study is conducted both quantitatively and qualitatively. Table 1 shows the variation in C_d with different mesh resolutions. As can be seen, with the resolution larger than 62k elements, the drag coefficient is unchanged for both Newtonian and yield stress fluids. Furthermore, Figure 4 shows the influences of mesh refinement on the yield surfaces defined as τ=τ_0. The yield lines tend to converge with 62k mesh elements. This mesh resolution is considered the most optimal (see the computational cost in Table I) and hence employed for our simulations.

3.4. Validation

Our computational approach is validated in this part. It is noted that the calculations are carried out with the Finite Volume Method (FVM) (in Ansys Fluent v14.5) and second-order discretization schemes. The variables are set converged at 10^{-8}.

The solid-like regions produced by a Bingham fluid at which it is unyielded (i.e., $\tau \leq \tau_0$) are presented in Figure 5. Despite the fact that we use a real material (i.e., kaolinite clay suspension), our results agree very well with those provided by an artificial fluid in Zisis and Mitsoulis [17]. Indeed, both observe that there are two types of the solid-like zone in the flow field pattern: one is moving with the flow (the so-called moving rigid zone) and one attaches to the obstacle (the so-called static rigid zone). Additionally, these zones are larger and tend to merge with others when the Bn_H increases ($Bn_H=\tau_0 H/Ku_0$).

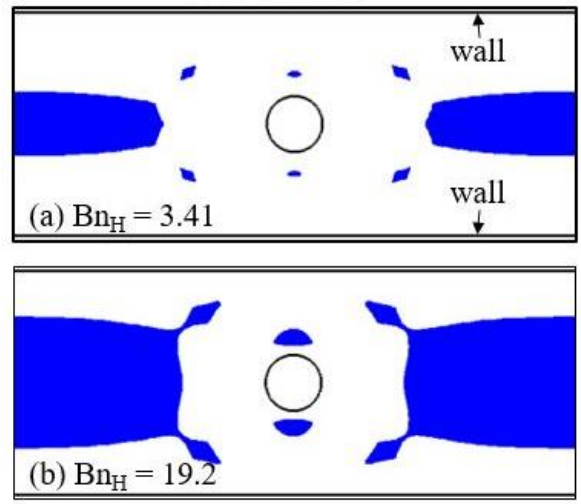

Figure 5. *Formation of solid-like regions (blue) at Re=0*

4. Results and Discussion

In this section, both far-field and near-field flow field patterns, and hydrodynamic forces of kaolinite suspensions 0-28.5% are discussed and analyzed in this section.

4.1. Far-field flow morphology

Results for the far-field flow morphology are shown in Figure 6. As can be seen, the far-field solid-like regions, which are of moving type, are formed in the channel core. These zones are observed to reduce in size as Re increases and/or kaolinite mass fraction decreases. It is worth noting that the effect of the kaolinite concentration on the size is more pronounced than that of Re (within the range investigated here). Specifically, the far-field rigid regions obtained by kaolinite 28.5% at Re=50 occupy almost the whole channel thickness (see Figure 6c), and those of 15% at Re = 100 are significantly thinner (see Figure 6a). It is also noticed that the shape of the solid-like region in the upstream shows the process of stabilizing after some distance from the inlet. This distance is found to be longer

for smaller kaolinite concentrations and/or at greater Re, e.g, longest for kaolinite 15% at Re=100 and shortest for kaolinite 28.5% at Re=50.

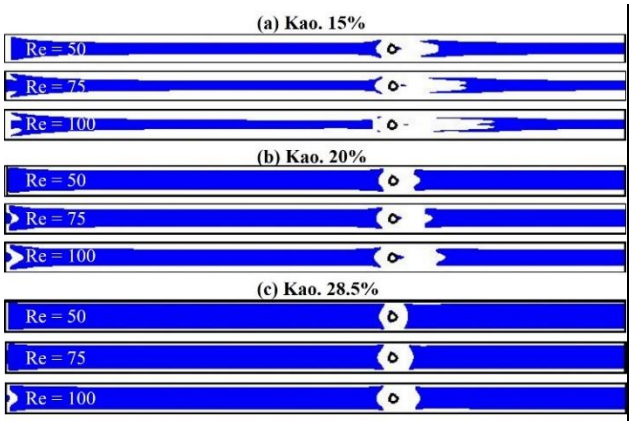

Figure 6. *Formation of far-field unyielded zones (blue) and yielded zones (white) at Re = 50-100*

Furthermore, as the solid-like zones get smaller, the flowing region, in which the fluid material is yielded, becomes greater. For instance, at Re=100, the flowing region produced by kaolinite 15% stretches to a distance of approximately 8*D* downstream whereas it is less than 1*D* with kaolinite 28.5% at Re=50.

4.2. Near-field flow pattern

In this part, near-field flow behaviors of kaolinite suspensions 0-28.5% over a confined cylinder are discussed and analyzed. Additionally, a comparison to the unconfined flow is provided to examine the effects of the channel wall proximity.

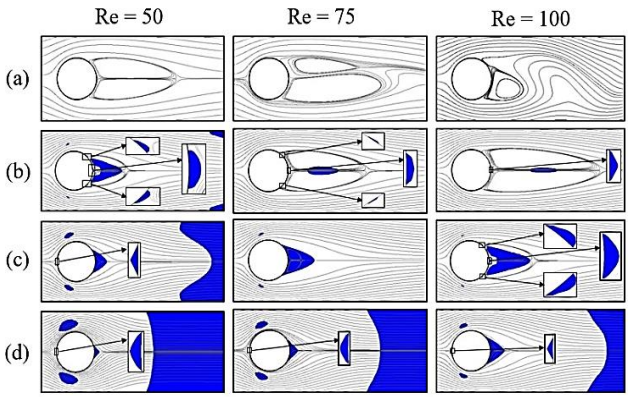

Figure 7. *Flow structures of a Newtonian fluid (a), kaolinite suspension 15% (b), 20% (c) and 28.5% in a confined channel at Re=50-100*

Simulation results for the flow streamlines and rigid zones are illustrated in Figure 7. It is evident that the flow structures of the yield stress fluid are greatly dependent on the kaolinite mass fraction (i.e., viscoplastic effect) and Reynolds number (i.e., inertial effect). For a Newtonian liquid, the flow is steady at Re=50 but exhibits non-stationary vortices downstream at Re=75 and 100; this agrees well with [10]. The suspension flows are, however, stationary in all the cases of kaolinite mass fraction studied in this work. With high concentration, e.g., *c*=28.5%, the flow is even in a creeping without any circulation bubbles formed downstream. This steady retention is attributable to the appearance of rigid zones, reducing the flowability and thus decreasing the inertial effect. These zones are observed to be further to the cylinder when Re increases and/or the kaolinite concentration decreases. Especially, with $c \geq 20\%$, the downstream solid-like zone created by the fluid flow adheres to and becomes an extending part of the cylinder; as Re increases, this zone is found to get larger. Furthermore, another static rigid zone can exist upstream when the kaolinite fraction is large (e.g., *c*=28.5%).

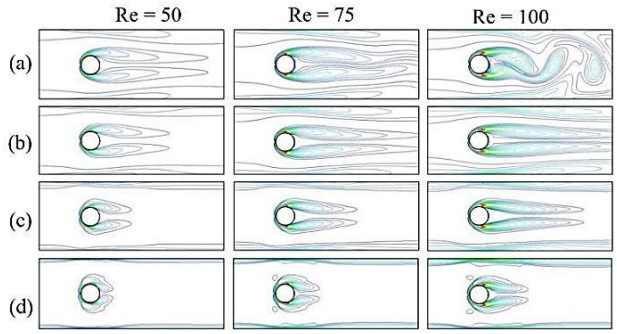

Figure 8. *Vorticity distribution of a Newtonian fluid (a), kaolinite suspension 15% (b), 20% (c) and 28.5% in a confined channel at Re = 50-100*

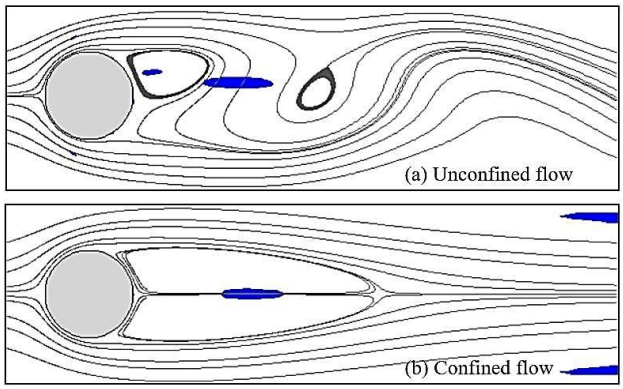

Figure 9. *Comparison in flow structures of kaolinite 15% between unconfined and confined cases at Re=100*

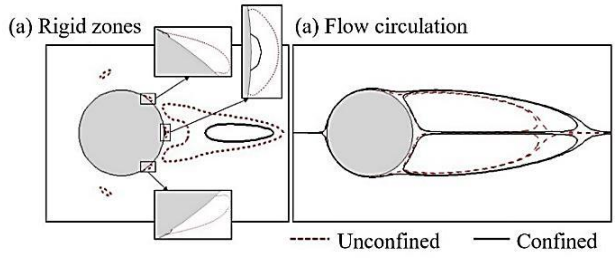

Figure 10. *Comparison in the rigid zones and downstream bubble of kaolinite 15% between unconfined and confined cases at Re=75*

Results for the vorticity contours of kaolinite 0-28.5% are presented in Figure 8. Two vortex structures are found on the lateral sides of the cylinder, emanating from the cylinder's surface. With the yield stress fluid, and for all the Re investigated, these structures are symmetrical with respect to the horizontal centerline. Moreover, they are stable, and longer for less viscous fluid. This agrees with the steady laminar regime of suspension flows in Figure 7. With the Newtonian fluid, these vortex structures are even longer they can interact with each other, alternately

separating from the cylinder's surface, thus resulting in the unsteady wake downstream at Re=75 and 100.

In addition, proximal channel walls are found to have considerable influences on the flow structures of a yield stress fluid flow. It is noted that the case of unconfined flow represents a very large blockage ratio (β=∞). Similar to findings for a Newtonian liquid, the wall proximity is also observed to stabilize the yield stress fluid flow. For example, the unconfined suspension flow of kaolinite 15% can transform to the non-stationary regime rather than still remaining in the stationary one for the confined case at Re=100 (see Figure 9).

Moreover, the blockage also significantly affects the formation of rigid zones and circulation bubbles (in a steady flow regime). For instance, at Re=75, the confined flow of kaolinite 15% produces less solid-like zones (i.e., no upper and lower moving rigid zones); the ones existing are considerably smaller and further to the cylinder than those created by the unconfined flow (see Figure 10a). Regarding to the circulation bubbles, their size increases for the confined case (see Figure 10b).

4.3. Hydrodynamic forces

In this part, results for drag force acting on the cylinder with different Re and kaolinite mass fractions are reported and analyzed. The drag coefficient is expressed as:

$$C_d = \frac{2F_d}{\rho u_0^{\,2} A}. \tag{8}$$

Here, F_d is drag force, A is the reference area.

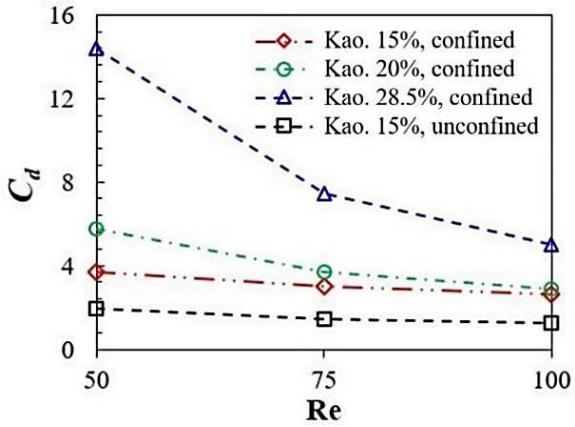

Figure 11. *Variation in C_d with different values of Re*

The drag strongly depends on Re and the yield stress (i.e., kaolinite concentrations) (see Figure 11). The effect of the latter is seen to be more obvious than the former. For the range of kaolinite fraction studied in this work, the larger Re, the smaller the drag coefficient acting on the cylinder. Moreover, when the kaolinite fraction is increased, C_d is dramatically increased. Indeed, at Re=50, the drag coefficient obtained by the suspension flow of kaolinite 28.5% is ~3.9 times larger than that of kaolinite 15%.

Furthermore, an approximation function for the drag coefficient exerted by a yield stress fluid flow for the blockage ratio of β = 4 can be proposed as follows:

$$C_d = 73.9(Re_{D,gen})^{-\frac{3}{4}} \tag{9}$$

with

$$\mathrm{Re}_{D,gen} = \frac{\rho u D}{(\tau_0/8)(D/u) + K(3m_e+1)/(4m_e)}, \tag{10}$$

$$m_e = \frac{K(8u/D)}{\tau_0 + K(8u/D)}. \tag{11}$$

Derivations for $\mathrm{Re}_{D,gen}$ can be referred to [24]. The curve the approximation function (Eq. (9)) is illustrated in Figure 12. It is good to observe that our results for a Newtonian fluid at $\mathrm{Re}_{D,gen}$=50, 75, and 100 have perfect match with those found by Biijam and Dhiman [16].

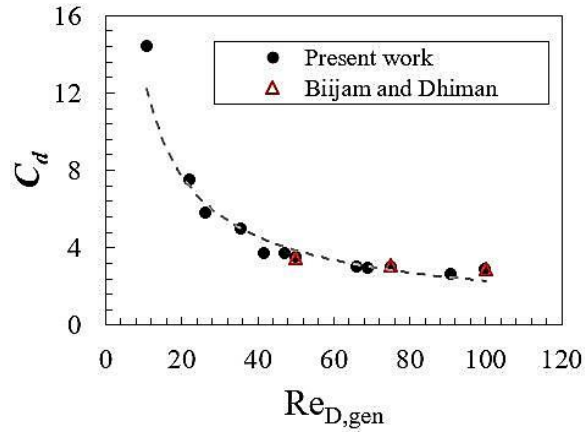

Figure 12. *C_d as the function of $Re_{D,gen}$*

5. Concluding remarks

In this work, hydrodynamic behaviors of the yield stress fluid over a cylinder confined in a channel were numerically investigated. The blockage ratio was β=4. The fluid was a water-sediment mixture with the kaolinite mass fraction varying from 15-28.5%. Reynolds number ranged from Re=50-100. The rheological modeling was carried out with Bingham and Papanastasious' regularization approaches.

The suspension flow was in a stationary regime in all the cases conducted; it was even seen to be in a creeping mode without circulation bubbles formed behind the cylinder with a high kaolinite fraction (i.e., c=28.5%). Moreover, the far-field solid-like zone was detected in the channel core; they were found to be larger, thereby narrowing the flowing zone, with the decreasing Re and/or increasing yield stress effect. The near-field solid-like zones were found around and/or on the cylinder; their formation was greatly dependent on the yield stress characteristics. Additionally, the confined flow was observed to provide different morphology, i.e., streamline pattern, vorticity distribution, and rigid regions, compared to the unconfined one.

The drag coefficient was varied with Re and yield stress effect. As Re decreased and/or kaolinite fraction increased, the drag significantly increased. A drag estimation function for the blockage ratio of β=4 was also proposed.

REFERENCES

[1] A. Shakeel, A. Kirichek, and C. Chassagne, "Yield stress measurements of mud sediments using different rheological methods and geometries: An evidence of two-step yielding", *Marine Geology*, vol. 427, 2020, pp. 106247.

[2] G. Hulme, "The interpretation of lava flow morphology", *Geophysical Journal International*, vol. 39, no. 2, 1974, pp. 361-383.

[3] P. Coussot, Q. D. Nguyen, H. T. Huynh, and D. Boon, "Avalanche behavior in yield stress fluids", *Physical Review Letters*, vol. 88, no. 17, 2002, pp. 175501.

[4] F. Mahmoodzadeh and S. E. Chidiac, "Rheological models for predicting plastic viscosity and yield stress of fresh", *Cement and Concrete Research*, vol. 49, 2013, pp. 1-9.

[5] G. Pangalos, J. M. Dealy, and M. B. Lyne, "Rheological properties of new inks", *Journal of Rheology*, vol. 29, no. 4, 1985, pp. 474-491.

[6] C. J. Dimitriou and G. H. McKinley, "A comprehensive constitutive law for waxy crude oil: a thixotropic yield stress fluid", *Soft Matter*, vol. 10, no. 35, 2014, pp. 6619-6644.

[7] F. K. Oppong, L. Rubatat, B. J. Frisken, A. E. Bailey, and J. R. Bruyn, "Microrheology and structure of a yield-stress polymer gel, *Physical Review E*, vol. 73, no. 4, 2006.

[8] J. Chakraborty, N. Verma, and Chhabra, "Wall effects in flow past a circular cylinder in a plane channel: A numerical study", *Chemical Engineering and Processing: Process Intensification*, vol. 43, no. 12, 2004, pp. 1529-1537.

[9] M. Sahin and R. G. Owens, "A numerical investigation of wall effects up to high blockage ratios on two-dimensional flow past a confined circular cylinder", *Physics of Fluids*, vol. 16, no. 5, 2004, pp. 1305-1320.

[10] S. Singha and K. Sinhamahapatra, "Flow past a circular cylinder between parallel walls at low Reynolds numbers", *Ocean Engineering*, vol. 37, no. 8-9, 2010, pp. 757-769.

[11] D. L. Tokpavi, A. Magnin, and P. Jay, "Very slow flow of Bingham viscoplastic fluid around a circular cylinder", *Journal of Non-Newtonian Fluid Mechanics*, vol. 154, no. 1, 2008, pp. 65-76.

[12] D. L. Tokpavi, P. Jay, A. Magnin, and L. Jossic, "Experimental study of the very slow flow of a yield stress fluid around a circular cylinder", *Journal of Non-Newtonian Fluid Mechanics*, vol. 164, no. 1-3, 2009, pp. 35-44.

[13] S. Mossaz, P. Jay, and A. Magnin, "Criteria for the appearance of recirculating and non-stationary regimes behind a cylinder in a viscoplastic fluid", *Journal of Non-Newtonian Fluid Mechanics*, vol. 165, 2010, pp. 1525-1535.

[14] S. Mossaz, P. Jay, and A. Magnin, "Non-recirculating and recirculating inertial flows of a viscoplastic fluid around a cylinder", *Journal of Non-Newtonian Fluid Mechanics*, vol. 177, 2012, pp. 64-75.

[15] R. P. Bharti, R. Chhabra, and V. Eswaran, "Two-dimensional steady Poiseuille flow of power-law fluids across a circular cylinder in a plane confined channel: Wall effects and drag coefficients", *Industrial & Engineering Chemistry Research*, vol. 46, no. 11, 2007, pp. 3820-3840.

[16] S. Biijjam and A.K. Dhiman, "CFD analysis of two-dimensional non-Newtonian power-law across a circular cylinder confined in a channel", *Chemical Engineering Communications*, vol. 199, no. 6, 2012, pp. 767-785.

[17] T. Zisis and E. Mitsoulis, "Viscoplastic flow around a cylinder kept between parallel plates", *Journal of Non-Newtonian Fluid Mechanics*, vol. 105, no. 1, 2002, pp. 1-20.

[18] E. Mitsoulis, "On creeping drag flow of a viscoplastic fluid past a circular cylinder: Wall effects", *Chemical Engineering Science*, vol. 59, no. 4, 2004, pp. 789-800.

[19] Y. Lin, N. Phan-Thien, J. B. P. Lee, and B. C. Khoo, "Concentration dependence of yield stress and dynamic moduli of kaolinite suspensions", *Langmuir*, vol. 31, no. 16, 2015, pp. 4791-4794.

[20] C. M. Bui, T.C. Nguyen-Le, N.A. Ho-Tran, and V.C. Nguyen, "Flow Characteristics of Sediment Suspension in a Two-Dimensional Channel with the Presence of an Elbow," 2020 *Applying New Technology in Green Buildings (ATiGB)*, 2021, pp. 87-93

[21] T.C. Papanastasiou, "Flows of materials with yield", *Journal of Rheology*, vol. 31, no. 5, 1987, pp. 385-404.

[22] R.B. Bird, G. Dai, and B.J. Yarusso, "The rheology and flow of viscoplastic materials", *Reviews in Chemical Engineering*, vol. 1, no. 1, 1983, pp. 1-70.

[23] S. Ookawara, K. Ogawa, N. Dombrowski, and E. Amooie-Foumeny, "Unified entry length correlation for Newtonian, power-law and Bingham fluids in laminar pipe flow at low Reynolds number", *Journal of Chemical Engineering of Japan*, vol. 33, no. 4, 2000, pp. 675-678.

[24] K. Madlener, B. Frey, and H. K. Ciezki, "Generalized Reynolds number for non-Newtonian fluids", *Progress in Propulsion Physics*, vol. 1, 2009, pp. 237-250.